Adaptive Modal Gain Equalization Techniques in Multi-Mode Erbium-Doped Fiber Amplifiers

Reza Nasiri Mahalati, Daulet Askarov, and Joseph M. Kahn, *Fellow, IEEE*

***Abstract*—We demonstrate two adaptive methods to equalize mode-dependent gain (MDG) in multi-mode erbium-doped fiber amplifiers (MM-EDFAs). The first method uses a spatial light modulator (SLM) in line with the amplifier pump beam to control the modal powers in the pump. The second method uses an SLM immediately after the MM-EDFA to directly control the modal powers in the signal. We compare the performance of the two methods applied to a MM-EDFA with a uniform erbium doping profile, supporting 12 signal modes in two polarizations. We show that root-mean-squared MDGs lower than 0.5 and 1 dB can be achieved in systems having frequency diversity orders of 1 and 100, respectively, while causing less than a 2.6-dB loss of mode-averaged gain.**

***Index Terms*—Mode-division multiplexing, multi-input multi-output (MIMO), multi-mode fiber (MMF), optical fiber amplifiers.**

I. Introduction

As long-haul single-mode fiber systems approach information-theoretic limits [1], [2], spatial multiplexing in multi-mode or multi-core fibers offers a possible route to higher throughput [3]. The properties of transmission fibers and fiber amplifiers are crucial to the ultimate feasibility of spatially multiplexed long-haul systems. In transmission fibers, low group delay spread minimizes receiver signal processing complexity [4], while large modal effective areas minimize nonlinear effects. In fiber amplifiers, low mode-dependent gain (MDG) minimizes the loss of capacity and the potential for outage [5].

Methods for equalizing MDG in multi-mode erbium-doped fiber amplifiers (MM-EDFAs) may be classified as fixed or adaptive. Among fixed methods, the erbium doping profile in the MM-EDFA may be optimized to minimize MDG [6], [7]. Alternatively, a phase mask may be placed in the pump beam to optimize the pump modal content, or may be placed in the output beam to provide mode-selective attenuation. Although such fixed methods can greatly reduce MDG when implemented perfectly, non-idealities in the erbium doping profile or in the pumping can lead to increased MDG [7].

While fixed methods are appealing for their simplicity, adaptive MDG equalization methods may be necessary for several reasons. First, adaptive methods may compensate for the aforementioned non-idealities in the doping profile or pumping and may track them if they change over time. Second, it is desirable to equalize not only the MDG in a single MM-EDFA, but also the MDG accumulated in the link prior to the MM-EDFA, which is not likely to be known *a priori*. Third, even if the MDG of each amplifier is constant, the coupled MDG of a link can vary over time, since it depends on phase-dependent mode coupling along the link [5].

Among adaptive MDG equalization methods, the pump beam modal content may be adjusted by passing several variable-power beams through phase masks and combining them using beam splitters [8]. The beam splitter losses make this method increasingly inefficient as the number of pump beams is increased, as might be required to accommodate an increasing number of signal modes.

We present two new methods for adaptive equalization of MDG in MM-EDFAs. The first method is to control the modal content of the pump using a spatial light modulator (SLM) placed in the pump path. This method is more power-efficient than the previous method of controlling the modal content of the pump [8] as it only requires one pump laser per pump polarization, independent of the number of signal modes. The second method directly equalizes MDG in the signal by placing an SLM immediately after the MM-EDFA.

Here, we study MM-EDFAs for signals spatially multiplexed in 12 modes (six spatial modes in two polarizations). By numerical solution of multi-mode rate equations, we compare MDGs obtained before and after optimizing the SLM using the two proposed equalization schemes. We show that the first scheme is more power-efficient, adapts faster and requires simpler power monitoring method, but cannot perform per-wavelength MDG equalization. Therefore, if the first scheme is used, wavelength-dependent gain needs to be controlled either in the MM-EDFA using gain-flattening filters [9], or elsewhere in the network using appropriately designed multi-mode dynamic gain equalizers. The second scheme can perform per-wavelength MDG equalization if it is used inside liquid crystal-on-silicon wavelength selective switches (LCOS WSSs) [10].

We study the impact of frequency-dependent MDG accumulated in the link before the MM-EDFA on these two MDG equalization schemes. By analyzing links with low and high frequency diversity orders [11], we show that the schemes remain highly effective even in the presence of highly frequency-dependent accumulated MDG.

The remainder of this paper is as follows. In Section II, we describe the mathematical model for a multi-span mode-division multiplexed system and quantify MDG in such systems.

Manuscript received November 3, 2013; revised December 31, 2013, February 2, 2014, and March 18, 2014; accepted March 19, 2014. Date of publication April 7, 2014; date of current version May 21, 2014. This work was supported by the National Science Foundation under Grant ECCS-1101905 and Corning, Inc.

The authors are with the E. L. Ginzton Laboratory, Department of Electrical Engineering, Stanford University, Stanford, CA 94305 USA (e-mail: rnasiri@stanford.edu; daskarov@stanford.edu; jmk@ee.stanford.edu).

Color versions of one or more of the figures in this paper are available online at http://ieeexplore.ieee.org.

Digital Object Identifier 10.1109/JLT.2014.2314746

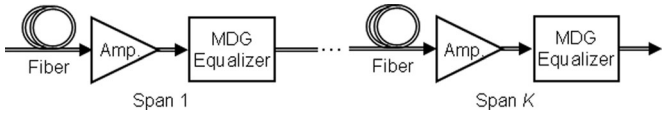

Fig. 1. Long-haul system with K spans, each including an amplifier and an (optional) equalizer for mode-dependent gain.

In Section III, we introduce our two methods for MDG equalization and describe the adaptive optimization algorithms used for each method. In Section IV, we give simulation results for the two techniques. We provide discussion and conclusions in Sections V and VI, respectively. We provide a detailed mathematical model of the MM-EDFA in the Appendix.

II. Quantifying MDG in a Multi-Span System

In order to describe MDG and modal dispersion in a long-haul mode-division multiplexed system, we model the link as the concatenation of numerous spans. Fig. 1 shows the block diagram of a system with K spans. Each span of multi-mode fiber (MMF) is followed by a MM-EDFA to compensate for the mode-averaged loss of the fiber. After each MM-EDFA there is an optional MDG equalizer that minimizes the root-mean-squared (RMS) MDG at the amplifier output. MDG from each amplifier depends weakly on frequency, but propagation makes MDG frequency-dependent [11] and hence, MDG is best equalized in or right after the MM-EDFA.

Assuming a MMF supporting D_{s} orthogonal propagating signal modes (including polarization and spatial degrees of freedom) and neglecting nonlinearity and noise, the total propagation operator of the multi-span system is a $D_{\mathrm{s}} \times D_{\mathrm{s}}$ matrix that multiplies complex baseband modal envelopes at frequency ω, and is given by

$$\mathbf{M}(\omega) = \prod_{k=1}^{K} \mathbf{M}_{\mathrm{eq}}^{(k)} \mathbf{\Lambda}_{\mathrm{amp}}^{(k)} \mathbf{M}_{\mathrm{fiber}}^{k}(\omega), \tag{1}$$

where $\mathbf{M}_{\mathrm{fiber}}^{(k)}(\omega), \mathbf{\Lambda}_{\mathrm{amp}}^{(k)}$ and $\mathbf{M}_{\mathrm{eq}}^{(k)}$ are the propagation operators of the MMF, the MM-EDFA and the MDG equalizer in the kth span, respectively. In (1), we assume MDG from the transmission fibers is negligible compared to that from the optical amplifiers [6], [12], [13].

$\mathbf{M}_{\mathrm{fiber}}^{(k)}(\omega)$ is a $D_{\mathrm{s}} \times D_{\mathrm{s}}$ unitary matrix that includes the effects of mode coupling and modal dispersion in the MMF. We model each fiber span as the concatenation of numerous short sections, each slightly longer than the length over which complex baseband modal fields remain correlated [14]. By decreasing the section length, thus increasing the number of sections, we can increase the strength of mode coupling. Throughout this paper, we assume the strong-coupling regime, where the number of independent sections is large compared to unity. It has been proven that in the strong-coupling regime, MDG accumulates with the square root of the number of sources and the statistics of the end-to-end MDG depend only on accumulated RMS MDG [5]. Also, strong mode coupling helps to minimize the spread of modal group delays, which is required to lower the receiver signal processing complexity [15]–[17]. It should be noted, however, that neither of our MDG equalization schemes depends on strong coupling to work. In fact, our methods work in systems where there is a combination of weak and strong coupling or no coupling at all. The MDG reduction obtained in such systems might be different from what we report here for a strongly coupled system.

Assuming each fiber span is a concatenation of N short sections, $\mathbf{M}_{\mathrm{fiber}}^{(k)}(\omega)$ is given by

$$\mathbf{M}_{\mathrm{fiber}}^{(k)}(\omega) = \prod_{l=1}^{N} \mathbf{V}_{\mathrm{fiber}}^{(k,l)} \mathbf{\Lambda}_{\mathrm{fiber}}(\omega) \mathbf{U}_{\mathrm{fiber}}^{(k,l)^{\mathrm{H}}}, \tag{2}$$

where $^{\mathrm{H}}$ denotes Hermitian conjugate. The $\mathbf{V}_{\mathrm{fiber}}^{(k,l)}$ and $\mathbf{U}_{\mathrm{fiber}}^{(k,l)}$ are frequency-independent $D_{\mathrm{s}} \times D_{\mathrm{s}}$ random unitary matrices representing mode coupling in the lth section of the kth MMF span. $\mathbf{\Lambda}_{\mathrm{fiber}}(\omega)$ is a $D_{\mathrm{s}} \times D_{\mathrm{s}}$ diagonal matrix that represents the uncoupled modal dispersion in one fiber section, which is assumed to be the same in all sections. It is given by

$$\mathbf{\Lambda}_{\mathrm{fiber}}(\omega) = \mathrm{diag}\Big(e^{-j\omega\tau_1}, \ldots, e^{-j\omega\tau_{D_s}}\Big), \tag{3}$$

where $\tau_1, \ldots, \tau_{D_{\mathrm{s}}}$ describe the uncoupled modal group delays in each MMF section.

The $\mathbf{\Lambda}_{\mathrm{amp}}^{(k)}$ is a frequency-independent $D_{\mathrm{s}} \times D_{\mathrm{s}}$ matrix representing MDG in the kth MM-EDFA. As it is shown is the Appendix, mode coupling is negligible in the MM-EDFA and hence $\mathbf{\Lambda}_{\mathrm{amp}}^{(k)}$ is a diagonal non-unitary matrix given by

$$\mathbf{\Lambda}_{\mathrm{amp}}^{(k)} = \mathrm{diag}\Big(e^{\frac{1}{2}g_1^{(k)}}, \ldots, e^{\frac{1}{2}g_{D_s}^{(k)}}\Big), \tag{4}$$

where $g_1^{(k)}, \ldots, g_{D_s}^{(k)}$ describe frequency-independent uncoupled modal power gains in the kth MM-EDFA.

$\mathbf{M}_{\mathrm{eq}}^{(k)}$ is a frequency-independent $D_{\mathrm{s}} \times D_{\mathrm{s}}$ matrix representing MDG and mode coupling in the kth equalizer. It is a non-diagonal and non-unitary matrix. If there are no separate equalizers in the system, $\mathbf{M}_{\mathrm{eq}}^{(k)}$ is the identity matrix.

The overall MDG operator of the system at a frequency ω is given by $\mathbf{M}(\omega)\mathbf{M}^{\mathrm{H}}(\omega)$. The eigenvectors of the MDG operator are the systems's spatial subchannels and its eigenvalues are the spatial subchannel gains. The overall MDG vector $\mathbf{g} = (g_1, \ldots, g_{D_s})$ is the vector of the logarithms of the eigenvalues of the MDG operator, which quantifies the overall MDG of the multi-input multi-output (MIMO) system.

As it was shown in [5], in strong-coupling regime, where $NK \gg 1$ and the $\mathbf{V}_{\mathrm{fiber}}^{(k,l)}$ and $\mathbf{U}_{\mathrm{fiber}}^{(k,l)}$ are all independent, the statistics of the end-to-end accumulated MDG are fully determined by RMS MDG in the kth span for $1 \le k \le K$. The RMS MDG in the kth span is the standard deviation of the MDG vector of the kth span, given by

$$\sigma_g^{(k)} = \mathrm{std}\Big(\log\Big(\mathrm{eig}\Big((\mathbf{M}_{\mathrm{eq}}^{(k)}\mathbf{\Lambda}_{\mathrm{amp}}^{(k)})(\mathbf{M}_{\mathrm{eq}}^{(k)}\mathbf{\Lambda}_{\mathrm{amp}}^{(k)})^{\mathrm{H}}\Big)\Big)\Big). \tag{5}$$

The end-to-end accumulated RMS MDG is given by the square root of

$$\xi^2 = \sum_{k=1}^{K} \sigma_g^{(k)}. \tag{6}$$

It was also shown in [5] that in the strong-coupling regime, when the overall MDG is small, the overall RMS MDG σ_{MDG} depends solely on the accumulated RMS MDG via

$$\sigma_{\mathrm{MDG}} = \xi\sqrt{1+\tfrac{1}{12}\xi^2}. \tag{7}$$

It is important to minimize accumulated RMS MDG ξ in a long-haul link, as a high accumulated RMS MDG will fundamentally limit the average capacity and outage capacity of the system [5]. Since in the strong-coupling regime, the accumulated MDG is fully determined by the MDG in each amplification node (as described by (6)), we can focus on minimizing the RMS MDG $\sigma_g^{(k)}$ in a single amplification node.

The MDG measured at the output of the kth amplification node reflects not only the MDG of the amplifier, but also the accumulated MDG in the link prior to the amplifier. Assuming $\mathbf{M}_{\mathrm{link}}^{1\to k}(\omega)$ is a $D_{\mathrm{s}} \times D_{\mathrm{s}}$ matrix representing the propagation operator of the link up to the kth amplifier, the MDG vector measured at the output of the kth amplification node (including the equalizer) is

$$\mathbf{g}^{(k)}(\omega) = \log(\mathrm{eig}((\mathbf{M}_{\mathrm{eq}}^{(k)}\,\mathbf{\Lambda}_{\mathrm{amp}}^{(k)}\mathbf{M}_{\mathrm{link}}^{1\to k}(\omega)) \times (\mathbf{M}_{\mathrm{eq}}^{(k)}\,\mathbf{\Lambda}_{\mathrm{amp}}^{(k)}\mathbf{M}_{\mathrm{link}}^{1\to k}(\omega))^{\mathrm{H}})). \tag{8}$$

Although the MDG $\sigma_g^{(k)}$ given by (5) is frequency-independent, the accumulated MDG from previous link spans is frequency-dependent due to propagation [11] and hence, the MDG vector measured at the output of each amplification node is generally frequency dependent. The kth amplifier RMS MDG $\sigma_g^{(k)}$ cannot be directly measured, but an empirical estimate of it can be found based on the measured MDG vector at the output of the kth amplification node. This estimate is given by

$$\hat{\sigma}_g^{(k)} = \left[\frac{1}{2\pi B}\int \mathrm{var}\left(\mathbf{g}^{(k)}(\omega)\right) d\omega\right]^{1/2}, \tag{9}$$

where B is the bandwidth in Hertz over which integration is performed, and can be equal to the bandwidth of one or many channels. Since we will be focusing on equalizing the MDG of a single amplification node, we drop the superscript $^{(k)}$ hereafter.

For the purpose of simulation, we can model the link propagation operator $\mathbf{M}_{\mathrm{link}}^{1\to k}(\omega)$ as having independent subchannels and independent identically distributed subchannel gains in F_D frequency bands, where F_D is the frequency diversity order of the link [11]. The frequency diversity order F_D is the ratio of the signal bandwidth to the coherence bandwidth of the subchannel gains, and is given approximately by the product of the symbol rate and the coupled RMS group delay [11]. We study two cases. The first case is $F_D = 1$, which corresponds to a frequency-independent accumulated MDG in the link prior to the MM-EDFA. The second case is $F_D = 100$ which corresponds to a highly frequency-dependent accumulated MDG in the link prior to the MM-EDFA.

In Section III we introduce two schemes for adaptive equalization of MDG in an amplification node. Each adaptive scheme requires $\hat{\sigma}_g$ to be measured at the output of MM-EDFA and uses it as an error signal to be minimized.

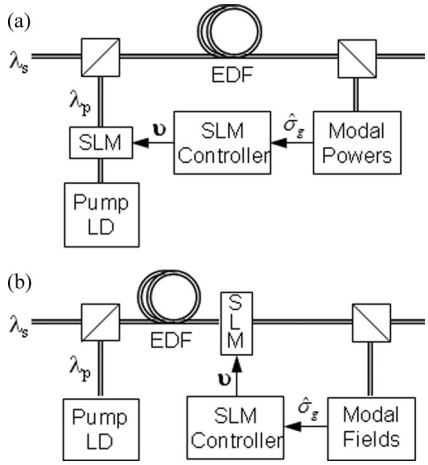

Fig. 2. (a) Block diagram of the system with SLM in line with the pump beam of the MM-EDFA. RMS MDG estimate is found using a modal power meter. The SLM controller uses and an adaptive algorithm to find the optimal SLM phases $\boldsymbol{\upsilon}$ such that is minimized. (b) Block diagram of the system with SLM at the amplifier output. Modal electric fields need to be coherently measured to extract RMS MDG estimate. The SLM controller uses and an adaptive algorithm to find the optimal SLM phases $\boldsymbol{\upsilon}$ such that is minimized.

The first scheme only involves a change in the MM-EDFA pump laser and does not require a separate equalizer. Since the MM-EDFA causes negligible mode coupling, the gains of spatial subchannels are equal to the power gains of signal modes. Therefore, in practice the MDG vector $\mathbf{g}(\omega)$ can be recovered from modal power measurements at different frequency bands and does not require coherent measurement of the modal fields. The empirical estimate of σ_g would then be given by (9).

The second scheme requires inserting an equalizer immediately after the MM-EDFA. Since the equalizer causes mode coupling, obtaining the empirical estimate of RMS MDG σ_g requires coherent detection of modal fields. The MDG vector $\mathbf{g}(\omega)$ can be calculated from modal field measurements at different frequency bands using MIMO signal processing. The empirical estimate of σ_g would then be found using (9).

In the following section we discuss the details of the two MDG equalization methods and the adaptive optimization algorithms used.

III. Adaptive MDG Equalization Methods

We propose two methods for adaptive equalization of MDG in MM-EDFAs. In the first method an SLM is added in line with the pump laser beam of the amplifier [(see Fig. 2(a)]. The SLM controls the modal content of the pump laser that is launched into the EDF. By properly choosing the phases of SLM pixels via an adaptive algorithm, the RMS MDG estimate $\hat{\sigma}_g$ at the amplifier output can be minimized. This method does not require a separate equalizer after the amplifier. In the second method, the MM-EDFA is not modified. Instead, an SLM placed immediately after the amplifier acts as an equalizer [see Fig. 2(b)]. The SLM is in line with the signal beam at the amplifier output and by properly choosing the phases of SLM pixels via an adaptive algorithm $\hat{\sigma}_g$ at the SLM output can be minimized.

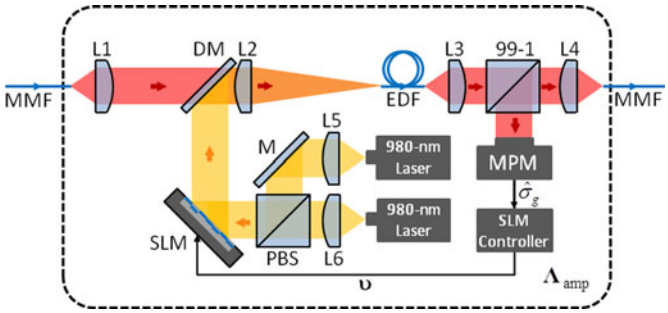

Fig. 3. MM-EDFA with SLM in the pump beam.

A. SLM in Pump Beam

Fig. 3 shows the detailed block diagram of our first proposed scheme for the adaptive control of MDG. Two orthogonally polarized pump lasers are combined using a polarizing beam splitter and illuminate a phase-only SLM. The beam reflected from the SLM is coupled into the EDF using a dichroic mirror (DM) and a lens. The SLM controls the electric field pattern of the pump at the input of the EDF. While it is possible to control each polarization separately, for simplicity, we control the two polarizations jointly, assuming a phase-only polarization-independent MEMS SLM. To first order, the amplifier gain is the same for pairs of degenerate modes that correspond to the LP modes in orthogonal polarizations; therefore, common control of both polarizations compensates MDG to first order.

At the output of the EDF, a small fraction (e.g., 1%) of the total power is redirected to a modal power meter (MPM). The MPM employs a mode demultiplexer and multiple power meters. The MPM extracts an error signal $\hat{\sigma}_g$ that is the empirical estimate of RMS MDG σ_g and passes it to the SLM controller. The SLM controller then uses the adaptive algorithm described in Section III-C to optimize the SLM phases υ such that the error signal is minimized and MDG is equalized.

Let $\mathbf{E}_{\mathrm{SLM,in}}(x,y)$ and $\mathbf{E}_{\mathrm{SLM,out}}(x,y)$ be the pump electric fields incident on and reflected form the SLM. The SLM comprises a two-dimensional array of reflective pixels. Assuming an SLM that has L square pixels with spacing $\Delta x = \Delta y$, we can discretize the (x,y) plane into a square grid of L pixels with the kth pixel centered at (x_k, y_k). The incident and reflected fields from SLM can then be represented as two vectors of length L, $\mathbf{E}_{\mathrm{SLM,in}}$ and $\mathbf{E}_{\mathrm{SLM,out}}$, whose kth entries are $\mathbf{E}_{\mathrm{SLM,in}}(x_k,y_k)$ and $\mathbf{E}_{\mathrm{SLM,out}}(x_k,y_k)$, respectively. Assuming the SLM is a specular reflector, we have

$$\mathbf{E}_{\mathrm{SLM,out}} = \mathbf{V}_{\mathrm{SLM}}\mathbf{E}_{\mathrm{SLM,in}}, \tag{10}$$

where V_{SLM} is a $L \times L$ diagonal matrix whose kth diagonal entry is the complex reflectance of the kth SLM pixel. For a phase-only SLM, the diagonal entries of V_{SLM} are

$$\mathbf{V}_{\mathrm{SLM},kk} = \upsilon_k = e^{j\varphi_k}, \qquad k = 1, \ldots, L \tag{11}$$

where φ_k is the phase of the kth SLM pixel.

If a linear optical device, such as a lens, is used to focus the pump electric field reflected from the SLM to the EDF input (see Fig. 3), propagation can be modeled by a linear operator ℓ (e.g., for a Fourier lens, ℓ is a Fourier transform). Thus, the pump electric field at the EDF input plane is

$$\mathbf{E}_{\mathrm{EDF,in,p}}(x_k,y_k) = \ell\left\{\mathbf{E}_{\mathrm{SLM,out}}(x_k,y_k)\right\}. \tag{12}$$

Assuming the EDF supports D_p modes at pump wavelength λ_p (including spatial and polarization degrees of freedom), we can expand the pump electric field at the EDF input in the basis of these propagating modes. Let $\mathbf{\Psi}_{\mathrm{p},i}(x,y)$ be the electric field corresponding to the ith propagating pump mode in the EDF. Then

$$\mathbf{E}_{\mathrm{EDF,in,p}}(x_k,y_k) = \sum_{i=1}^{D_p} a_{\mathrm{p},i}\mathbf{\Psi}_{\mathrm{p},i}(x_k,y_k) + \text{radiation modes}. \tag{13}$$

Assuming the EDF is a weakly guiding fiber, where $\mathbf{\Psi}_{\mathrm{p},i}(x,y)$ can assumed to be transverse, the expansion coefficients $a_{\mathrm{p},i}$ can be approximated by the following inner product

$$a_{\mathrm{p}.i} \approx \Delta x \Delta y \sum_{k=1}^{L} \mathbf{E}_{\mathrm{EDF,in,p}}(x_k,y_k)\cdot\mathbf{\Psi}^*_{\mathrm{p},i}(x_k,y_k). \tag{14}$$

Knowing the modal content of the pump electric field (i.e. the $a_{\mathrm{p},i}$'s) and the modal content of the signal electric field at the EDF input, the multi-mode rate equations can be numerically solved to find the gains of different signal modes at the EDF output (i.e. the MDG vector $\mathbf{g}(\omega)$), the details of which are discussed in the Appendix. In this scheme MDG equalization happens inside the MM-EDFA and there is no separate equalizer after the amplifier, therefore the amplifier RMS MDG is

$$\sigma_g = \mathrm{std}\Big(\log\left(\mathrm{eig}\left(\mathbf{\Lambda}_{\mathrm{amp}}\mathbf{\Lambda}^{\mathrm{H}}_{\mathrm{amp}}\right)\right)\Big). \tag{15}$$

Since $\mathbf{\Lambda}_{\mathrm{amp}}$ is a diagonal matrix, the eigenvalues of the amplifier gain operator are equal to the powers of individual signal modes in this case. Therefore, in practice the MDG vector $\mathbf{g}(\omega)$ can be measured using a MPM that consists of a mode demultiplexer and multiple power meters. The power meters recover $\mathbf{g}(\omega)$ by measuring the modal powers at different frequency bands. The error signal $\hat{\sigma}_g$ passed to the SLM controller is the empirical estimate of the amplifier RMS MDG σ_g and is calculated using (9). Details of the adaptive algorithm that the SLM controller uses to find the optimal SLM phases $\boldsymbol{\upsilon}$ that minimize the error signal $\hat{\sigma}_g$ are given in Section III-C.

Since the phase shifts of the MEMS SLM depend weakly on frequency, this scheme cannot perform per-wavelength MDG equalization. However, as mentioned before, the MDG in the amplifier depends weakly on frequency and hence, minimizing the frequency-averaged $\hat{\sigma}_g$ also minimizes $\hat{\sigma}_g$ at any single frequency.

B. SLM at Amplifier Output

Fig. 4 shows the detailed block diagram of our second proposed scheme for the adaptive control of MDG. Here the MM-EDFA remains unchanged. Two orthogonally polarized pumps are combined using a polarizing beam splitter and are coupled into the EDF using a DM and a lens. The signal beam at the amplifier output is focused onto a phase-only SLM using a lens. The beam reflected from the SLM is coupled into

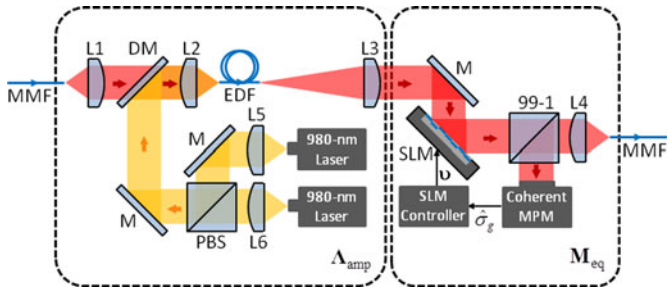

Fig. 4. MM-EDFA with SLM at the output.

a MMF using a lens. The SLM controls the modal content of the signal electric field that is coupled into the MMF. While it is possible to control each polarization separately, for simplicity, we control the two polarizations jointly, assuming a phase-only polarization-independent MEMS SLM. To first order, the amplifier gain is the same for pairs of degenerate modes that correspond to the LP modes in orthogonal polarizations; therefore, common control of both polarizations compensates MDG to first order.

At the output of the SLM, a small fraction (e.g., 1%) of the total power is redirected to a coherent MPM. The coherent MPM employs a mode demultiplexer and multiple coherent receivers. From coherent modal field measurements, the coherent MPM extracts the error signal $\hat{\sigma}_g$ using MIMO signal processing and passes it to the SLM controller. The SLM controller then uses the adaptive algorithm described in Section III-C to optimize the SLM phases $\boldsymbol{\upsilon}$ such that the error signal is minimized and MDG is equalized.

Let $\mathbf{E}_{\text{SLM,in}}$ and $\mathbf{E}_{\text{SLM,out}}$ be two vectors of length L representing electric fields incident on and reflected from the SLM discretized on a square grid of L pixels with spacing $\Delta x = \Delta y$. The relationship between $\mathbf{E}_{\text{SLM,in}}$ and $\mathbf{E}_{\text{SLM,out}}$ is given by (10). Note that here $\mathbf{E}_{\text{SLM,in}}$ and $\mathbf{E}_{\text{SLM,out}}$ represent signal electric fields whereas in Section III-A they were used to represent pump electric fields (compare Fig. 3 and Fig. 4). If linear optical devices, such as lenses, are used to focus the signal electric field from the EDF output onto the SLM, and focus reflected electric field from the SLM to the MMF input (see Fig. 4), propagation can be modeled by a linear operator ℓ (e.g., for a Fourier lens, ℓ is a Fourier transform). Thus, if $\mathbf{E}_{\text{EDF,out,s}}(x_k, y_k)$ is the signal electric field at the EDF output plane, we have

$$\mathbf{E}_{\text{SLM,in}}(x_k, y_k) = \ell\left\{\mathbf{E}_{\text{EDF,out,s}}(x_k, y_k)\right\}. \tag{16}$$

Also, the signal electric field at the MMF input plane after the amplifier is

$$\mathbf{E}_{\text{MMF,in}}(x_k, y_k) = \ell\left\{\mathbf{E}_{\text{SLM,out}}(x_k, y_k)\right\}. \tag{17}$$

Assuming the EDF and MMF support D_{s} modes at signal wavelength λ_{s} (including spatial and polarization degrees of freedom), and assuming L3 and L4 are Fourier lenses in Fig. 4 (not drawn to scale), we can expand the signal electric fields at the SLM plane in the basis of the Fourier transforms of these propagating modes. Let $\tilde{\mathbf{\Psi}}_{\text{s},i}(x, y)$ be the Fourier transform of the electric field corresponding to the ith propagating signal mode in the EDF and MMF. Then

$$\mathbf{E}_{\text{SLM,in}}(x_k, y_k) = \sum_{i=1}^{D_s} a_{\text{s},i}\, \tilde{\mathbf{\Psi}}_{\text{s},i}(x_k, y_k), \tag{18}$$

where the expansion coefficients $a_{\text{s},i}$ can be approximated by the following inner product

$$a_{\text{s}.i} \approx \Delta x \Delta y \sum_{k=1}^{L} \mathbf{E}_{\text{SLM,in}}(x_k, y_k) \cdot \tilde{\mathbf{\Psi}}^{*}_{\text{s},i}(x_k, y_k). \tag{19}$$

Similarly we have

$$\mathbf{E}_{\text{SLM,out}}(x_k, y_k) = \sum_{i=1}^{D_s} b_{\text{s},i}\, \tilde{\mathbf{\Psi}}_{\text{s},i}(x_k, y_k) + \text{radiation modes}, \tag{20}$$

where the expansion coefficients $b_{\text{s},i}$ can be approximated by the following inner product

$$b_{\text{s}.i} \approx \Delta x \Delta y \sum_{k=1}^{L} \mathbf{E}_{\text{SLM,out}}(x_k, y_k) \cdot \tilde{\mathbf{\Psi}}^{*}_{\text{s},i}(x_k, y_k). \tag{21}$$

Thefore, neglecting the radiation modes, the incident and reflected signal electric fields on the SLM plane can be represented by state vectors $\boldsymbol{A}_{\text{s}}$ and $\boldsymbol{B}_{\text{s}}$, which are column vectors of the expansion coefficients $a_{\text{s},i}$ and $b_{\text{s},i}$, respectively. In the basis of the Fourier transforms of signal modes, the relationship between the signal electric fields incident on and reflected from the SLM can therefore be written as

$$\mathbf{B}_s = \mathbf{M}_{\text{eq}} \mathbf{A}_s, \tag{22}$$

where $\boldsymbol{M}_{\text{eq}}$ is the equalizer operator and is related to the SLM reflectance matrix $\boldsymbol{V}_{\text{SLM}}$ by

$$\mathbf{M}_{\text{eq}} = \mathbf{U}_{\text{mode}} \mathbf{V}_{\text{SLM}} \mathbf{U}^{\text{H}}_{\text{mode}}, \tag{23}$$

where $\mathbf{U}_{\text{mode}}$ is a $D_{\text{s}} \times L$ semi-unitary matrix whose rows are given by the Fourier transforms of the propagating signal modes reshaped into row vectors, i.e.

$$\mathbf{U}_{\text{mode}} = \begin{pmatrix} \tilde{\mathbf{\Psi}}_{\text{s},1}(x_k, y_k) \\ \vdots \\ \tilde{\mathbf{\Psi}}_{\text{s},D_s}(x_k, y_k) \end{pmatrix}. \tag{24}$$

In this scheme we have an equalizer after the MM-EDFA and the RMS MDG of the amplification node is

$$\sigma_g = \text{std}\Big(\log\Big(\text{eig}\Big((\mathbf{M}_{\text{eq}}\mathbf{\Lambda}_{\text{amp}})(\mathbf{M}_{\text{eq}}\mathbf{\Lambda}_{\text{amp}})^{\text{H}}\Big)\Big)\Big). \tag{25}$$

Note that although V_{SLM} is a diagonal matrix, M_{eq} is generally non-diagonal. Hence, using the SLM as an equalizer after the MM-EDFA will cause the signal modes to couple. Due to this mode coupling caused by the SLM, in practice signal electric fields need to be coherently detected after the SLM to recover the MDG vector $\mathbf{g}(\omega)$. The coherent MPM in Fig. 4 first demultiplexes the modes and coherently detects the electric fields in all signal modes. It then uses a $D_{\text{s}} \times D_{\text{s}}$ MIMO equalizer to estimate the inverse of the channel matrix $\mathbf{M}(\omega)$. The MIMO equalization can be done either in the time or the frequency domain [18]–[20]. However, frequency domain equalization is

more efficient [20]. From the estimate of the inverse of the channel matrix $\mathbf{M}(\omega)$, the MDG vector $\mathbf{g}(\omega)$ can be calculated at different frequency bands. The error signal $\hat{\sigma}_g$ passed to the SLM controller is then calculated using (9). Details of the adaptive algorithm that the SLM controller uses to find the optimal SLM phases $\boldsymbol{\upsilon}$ that minimize the error signal $\hat{\sigma}_g$ are given in the next section.

Although this method cannot perform per-wavelength MDG equalization as described here, the same idea can be applied to a LCOS WSS to perform per-wavelength MDG equalization [10].

C. Adaptive Optimization Algorithms

In practice, an adaptive algorithm is employed to find the optimal SLM reflectances that minimize the error signal. In such an algorithm, at each step, one or a few SLM reflectances are updated based on some measurements of the error signal. If a phase-only SLM is used, the reflectances to be optimized are of the form $\upsilon_k = e^{j\varphi_k}$, where the φ_k are the phases of the SLM pixels. In practice, to reduce the number of optimization variables, multiple pixels can be grouped into larger disjoint square blocks where the phase over each block is constant. As discussed in the next section, the optimum number of blocks for the two MDG equalization methods are different.

Since the RMS MDG σ_g at the output of an amplification node cannot be directly measured while doing MDG equalization, we choose the error signal to be $\hat{\sigma}_g$, the empirical estimate of σ_g. As it is shown in the previous sections and the Appendix, for both of our proposed MDG equalization methods, $\hat{\sigma}_g$ has a complicated dependence on the SLM reflectances and cannot be written or even approximated in a closed mathematical form. This prevents us from using continuous-phase sequential coordinate ascent (CPSCA) algorithms that work very efficiently for the problems where the error signal has a simple mathematical dependence on the optimization variables [21], [22].

For the case of having the SLM in the pump beam, after trying different optimization algorithms, we found that an effective algorithm to use is the four-phase sequential coordinate ascent (4PSCA). In this algorithm, at each step a single SLM block is chosen, and its phase is optimized over the set $\{0, \pi/2, \pi, 3\pi/2\}$ to minimize the error signal$\hat{\sigma}_g$. Then the next SLM block is selected and the process is repeated. In all our simulations the algorithm converged after one pass over the SLM blocks.

For the case of having the SLM after the amplifier, after trying different optimization algorithms, we found that an effective algorithm to use is the randomized sequential coordinate ascent (RSCA). In this algorithm, at each step a single SLM block is chosen, and its phase is optimized over a set of eight random values, uniformly drawn from the interval $[0, 2\pi)$, to minimize the error signal $\hat{\sigma}_g$. If none of the eight random phase values leads to a $\hat{\sigma}_g$ smaller than its current value, the phase of the block remains unchanged. Then the next SLM block is selected and the process is repeated. According to our simulations, this algorithm requires multiple passes over the SLM to converge, but leads to a much lower equalized RMS MDG compared to other optimization algorithms for this scheme.

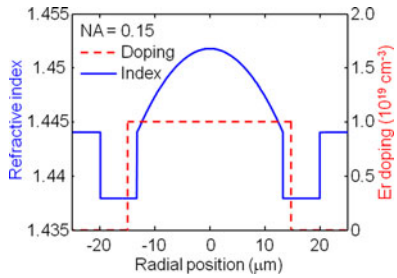

Fig. 5. Refractive index and erbium doping profile of the EDF.

We have verified through simulation that for both 4PSCA and RSCA, the order in which the SLM blocks are optimized does not affect the convergence rate of the algorithm or the final results. The results presented in Section IV were obtained by optimizing the SLM blocks from top-left to bottom right, but optimizing the blocks in any other order would lead to identical results.

Thus far, we described our two methods for MDG equalization, and the adaptive optimization algorithms used with each method. In the following section we give the simulation results for our two proposed methods.

IV. Simulation Results

In simulations, we take the input signal to be continuous-wave at a single wavelength $\lambda_s = 1550$ nm. The MMF and EDF both support $D_s = 12$ modes (6 spatial modes in each polarization) and we assume there is a power of 0.16 mW in each of the signal modes at the input of MM-EDFA. The pump wavelength is $\lambda_p = 980$ nm, and the EDF supports $D_p = 42$ pump modes at this wavelength. The pump power is chosen to be 1.5 W in order to yield initially a mode-averaged signal gain of 25 dB. The amplifier length is chosen to be the value of z at which the amplified signal power reaches its maximum, which turned to be 6.9 m for our choice of amplifier parameters. The EDF and MMF both have a graded-index, depressed cladding (GIDC) profile with 13.2-μm core radius, NA $= 0.15$ and the EDF has a uniform 10^{19} cm^{-3} erbium concentration up to a 14.6-μm radius. Fig. 5 shows the refractive index and erbium doping profile of the EDF. The graded index in EDF and MMF reduces the group delay spread of the modes and helps to reduce receiver signal processing complexity [17] while the depressed cladding reduces bending losses in the MMF and RMS MDG in the amplifier [6]. Although the uniform erbium doping profile is not optimized [6], it greatly simplifies the fabrication of the MM-EDFA. The effect of polarization-dependent loss is neglected in the simulations and hence, degenerate modes in the two polarizations experience identical gains.

We assume a 128 $\times$ 128-pixel phase-only MEMS SLM is used. Each pixel is 18 $\times$ 18 μm^2, with a phase controllable from 0 to 2π with 8-bit resolution.

To model the effect of accumulated MDG from link spans prior to the amplifier, that has become frequency-dependent after propagation [11], we assume the link propagation operator $\mathbf{M}_{\text{link}}^{1\to k}(\omega)$ has independent subchannels and independent

identically distributed subchannel gains in F_D frequency bands. We simulate the cases of frequency-independent accumulated MDG in the link ($F_D = 1$), and highly frequency-dependent accumulated MDG in the link ($F_D = 100$). For both cases we assume the accumulated RMS MDG from previous spans is $\xi = 5$ dB, which corresponds to 20 link spans prior to the amplifier, each with a residual RMS MDG of 1.1 dB. For the case of $F_D = 100$, we generate 100 independent link propagation matrices $\mathbf{M}_{\text{link}}^{1\to k}$, each having an accumulated RMS MDG $\xi = 5$ dB. However, since the amplifier MDG depends weakly on frequency, we use the same amplifier propagation operator $\mathbf{\Lambda}_{\text{amp}}$ for all the 100 frequency subchannels.

The error signal that we minimize is $\hat{\sigma}_g$, the empirical estimate of the RMS MDG of the amplification node, and it reflects both the MDG in the amplification node and the accumulated MDG in the link prior to the amplifier. However, we are interested to know by how much we can reduce the amplifier RMS MDG σ_g while adapting the SLM to minimize its empirical estimate $\hat{\sigma}_g$. Therefore, our simulation results show the actual amplifier RMS MDGs before and after equalization, denoted by $\sigma_{g,\text{uneq}}$ and $\sigma_{g,\text{eq}}$, respectively. In the following subsections we give the simulation results for our two MDG equalization methods.

A. SLM in Pump Beam

In simulations of our first MDG equalization method, we use a combination of two means to introduce different MDGs in the MM-EDFA. We change the focal lengths of the lenses L5 and L6 in Fig. 3 from their nominal value of $f = 10.4$ mm to change the beam waist of the pump laser and generate different MDGs in the amplifier. We also introduce some misalignment between the SLM and the EDF in Fig. 3 to generate different MDGs in the amplifier. For each beam waist, the size of the SLM blocks are chosen such that a set of 8×8 blocks covers a circle enclosing more than 95% of the energy incident on the SLM, so only these 64 blocks are adapted. The focal lengths of the lenses L1-L4 in Fig. 3 are all chosen to be $f = 5.0$ mm and are held constant throughout the simulations. We use the 4PSCA algorithm described in Section III-C to find the optimal the SLM phases.

Fig. 6 shows the equalized RMS MDG and the mode-averaged gain (MAG) of the MM-EDFA versus the unequalized RMS MDG, with the SLM in the pump beam. Each point in the figure is an average of 16 simulations with the same unequalized MDG. For a link with a frequency diversity order $F_D = 1$ [see Fig. 6(a)], the worst-case RMS MDG of 2.9-dB can be reduced to 0.6-dB while there would be a 2-dB reduction in MAG. For a link with a frequency diversity order $F_D = 100$ [see Fig. 6(b)], the worst-case RMS MDG of 2.9-dB can be reduced to 1-dB while there would be a 2.6-dB reduction in MAG. The reduced MAG at higher unequalized MDGs results from a reduction in pump coupling efficiency as the pump beam waist and alignment changes, and can be compensated by an increase in pump power. We see that the MDG equalization scheme is effective even in the presence of highly frequency-dependent accumulated MDG from the link.

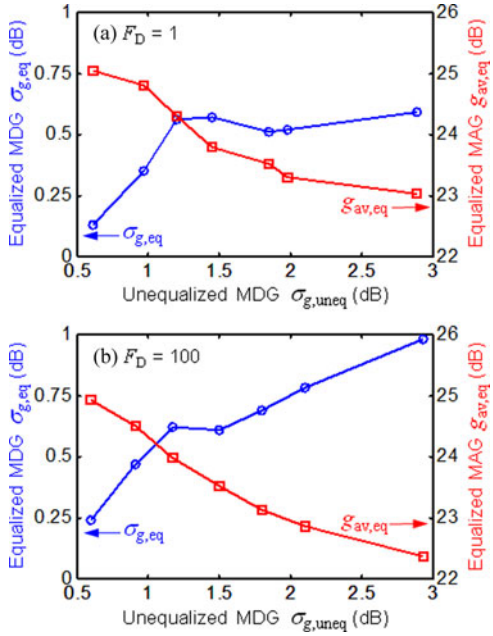

Fig. 6. Equalized RMS MDG and equalized MAG at the amplifier output, using SLM in pump beam. (a) No frequency diversity in accumulated MDG, (b) High frequency diversity in accumulated MDG.

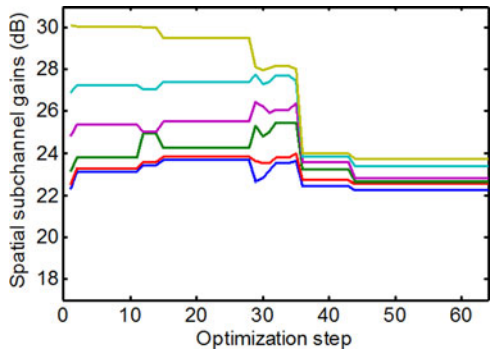

Fig. 7. Gains of six spatial subchannels in one polarization at the output of the MM-EDFA as a function of the optimization step with the SLM in pump beam. The gains converge after one optimization pass over the SLM blocks.

Fig. 7 shows the gains of the six spatial subchannels in one polarization measured at the output of the MM-EDFA as a function of the optimization step, for an sample case with $F_D = 1$. It is seen that the gains converge after one optimization pass over the 64 SLM blocks.

B. SLM at Amplifier Output

In simulations of our second MDG equalization method, it is not required to physically model the MM-EDFA. We randomly choose a set of modal gains for signals at the output of the amplifier according to distributions we obtained from previous amplifier simulations. We group SLM pixels into 32×32 square blocks, each comprising 4×4 pixels. The blocks cover a circle enclosing more than 95% of the energy incident on the SLM, so only these 1024 blocks are adapted. The focal lengths of the lenses L3 and L4 in Fig. 4 are chosen to be $f = 5.0$ mm and are not changed throughout the simulations. We use the RSCA

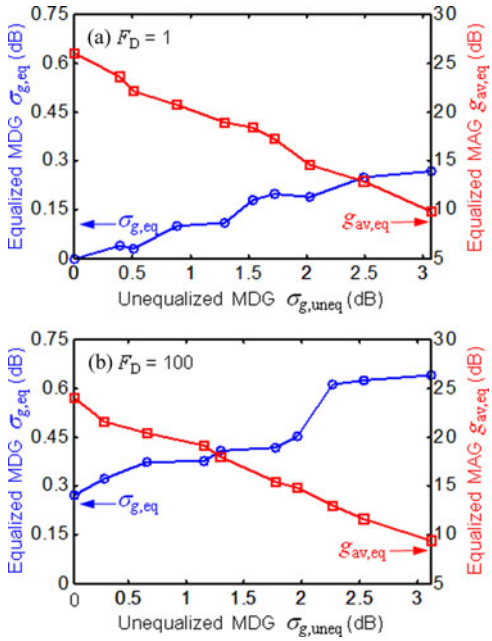

Fig. 8. Equalized RMS MDG and equalized MAG using the SLM after the amplifier. (a) No frequency diversity in accumulated MDG, (b) High frequency diversity in accumulated MDG.

algorithm described in Section III-C to find the optimal SLM phases.

Fig. 8 shows the equalized RMS MDG and MAG at the SLM output versus the unequalized RMS MDG, with the SLM at the amplifier output. Each point in the figure is an average of 16 simulations with the same unequalized MDG. For a link with a frequency diversity order $F_D = 1$ [see Fig. 7(a)], the worst-case RMS MDG of 3 dB can be reduced to less than 0.3 dB, while there is a 15-dB reduction in MAG. For a link with a frequency diversity order $F_D = 100$ [see Fig. 7(b)], the worst-case RMS MDG of 3 dB can be reduced to 0.65 dB, while there is a 16-dB reduction in MAG. The large reduction in MAG at higher unequalized MDGs results from the fact that the SLM is a passive device and the best it can do is to attenuate all the modes at the amplifier output to the level of the mode that experienced the smallest gain in the MM-EDFA. In the worst-case RMS MDG of 3 dB for instance, the mode with the lowest gain has a power gain of 18 dB and hence, even with an ideal equalizer a MAG loss of 7 dB is inevitable. We see that the MDG equalization is effective even in the presence of highly frequency-dependent accumulated MDG in the link.

Fig. 9 shows the gains of the six spatial subchannels in one polarization measured at the output of the MM-EDFA as a function of the optimization step, for a sample case with $F_D = 1$. It is seen that the gains converge after six optimization passes over the 1024 SLM blocks.

V. Discussion

MDG equalization using the SLM in the pump beam requires a simple power monitoring that involves a modal demultiplexer and multiple power meters to estimate the RMS MDG and pass it to the SLM controller as an error signal. This method is more

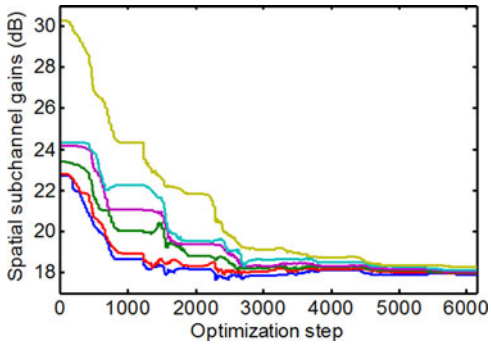

Fig. 9. Gains of six spatial subchannels in one polarization at the output of the MM-EDFA as a function of the optimization step with the SLM at amplifier output. The gains converge after six optimization passes over the SLM blocks.

scalable and efficient than previously proposed methods for controlling the modal content of the pump laser in a MM-EDFA that use several discrete pump modes [8]. Also, this method is more efficient than our second proposed method that uses the SLM after the amplifier, and can make moderate MDG very small with only a small reduction in MAG. Adaptation of SLM phases converges in one pass in this method. However, this technique cannot perform per-wavelength gain equalization.

MDG equalization using the SLM after the amplifier on the other hand, would require a complex monitoring that involves a modal demultiplexer, coherent receivers and a MIMO equalizer. Although this method can make moderate MDG very small even when there is high frequency diversity in the link, it is less efficient than placing the SLM in the pump beam and causes a large reduction in MAG. In this method, SLM adaptation converges after several passes. This method can perform per-wavelength gain equalization if used in LCOS WSSs [10].

VI. Conclusion

In a long-haul mode-division-multiplexed systems, a large accumulated end-to-end RMS MDG causes a loss of capacity and increases the potential for outage and hence it is essential to equalize MDG is such systems. MM-EDFAs are expected to be the main source of MDG in these systems. Although the MDG from each amplifier varies slowly over frequency, propagation through the MMF makes MDG vary rapidly over frequency [11]. Therefore, MDG is best equalized in or immediately after the MM-EDFAs.

We have proposed two methods for adaptive equalization of MDG in MM-EDFAs.

Our first method uses an SLM in the pump beam to control the modal content of the pump beam of the MM-EDFA. This method is more power efficient than previously proposed methods for controlling the modal content of the pump. We showed that this method can equalize an RMS MDG of 2.9 dB to less than 0.5 dB and less than 1 dB in links a having a frequency diversity order of 1 and 100, respectively, while causing less than 2.6-dB reduction in MAG in a MM-EDFA that supports 12 signal modes at 1550 nm.

Our second method places an SLM at the output of the MM-EDFA to directly equalize modal powers. We showed that

this method can equalize an RMS MDG of 3 dB to less than 0.3 dB and less than 0.7 dB in links a having a frequency diversity order of 1 and 100, respectively, while causing less than 16-dB reduction in MAG in a MM-EDFA that supports 12 signal modes at 1550 nm.

Our results show that while these two methods perform frequency-independent equalization of MDG, both are effective in the presence of highly frequency-dependent MDG accumulated in the link.

APPENDIX

The physical model that we use to describe the MM-EDFA is based on coupled mode theory [23] and rate equations of the erbium ion level populations [24] extended to account for multiple spatial modes. Using this model, we also show that mode coupling is negligible in MM-EDFA for both signal and pump modes.

Assuming there are no backward-propagating modes and neglecting noise, coupled wave equations for signal modes and pump modes in MM-EDFA would be

$$\frac{da_{\mathrm{s},k}}{dz} = -j\beta_{\mathrm{s},k}a_{\mathrm{s},k} + \gamma_{\mathrm{s},kk}(z)a_{\mathrm{s},k} + \sum_{l\neq k}\gamma_{\mathrm{s},kl}(z)a_{\mathrm{s},l}, \quad (26)$$

$$\frac{da_{\mathrm{p},m}}{dz} = -j\beta_{\mathrm{p},m}a_{\mathrm{p},m} + \gamma_{\mathrm{p},m}(z)a_{\mathrm{p},m}, \quad (27)$$

where $a_{\mathrm{s},k}$, $a_{p,m}$, $\beta_{\mathrm{s},k}$ and $\beta_{p,m}$ are the complex amplitudes and propagation constants of the kth signal mode and mth pump mode, respectively; $\gamma_{\mathrm{s},kl}$ is the coupling coefficient from the lth to the kth signal mode; $\gamma_{p,m}$ is the gain coefficient of the mth pump mode.

Here, we have included the coupling terms only for the signal modes. It will be shown that these terms have a negligible effect. Using the same argument we can show that the coupling terms for pump modes are negligible as well.

Using expansion in terms of ideal modes and assuming $|\gamma_{\mathrm{s},kl}| \ll |\beta_{\mathrm{s},kl}|$ and $|\varepsilon - \varepsilon_{ul}| \ll |\varepsilon|$, where ε is the complex dielectric constant of the medium and ε_u is the unperturbed dielectric constant of the medium in the absence of light, the expression for $\gamma_{\mathrm{s},kl}$ including the case $k = l$ is

$$\gamma_{\mathrm{s},kl} = (\omega\varepsilon_0/4jP)\int_{-\infty-}^{\infty}\int_{\infty}^{\infty}(\varepsilon - \varepsilon_u)\,\mathbf{E}^*_{\mathrm{s},k}\cdot\mathbf{E}_{\mathrm{s},l}\,dx\,dy, \quad (28)$$

where P is the power of a normalized mode and $\mathbf{E}_{\mathrm{s},k}$ is the normalized vector electric field distribution of the kth signal mode.

To express (26), (27) and (28) in terms of amplifier parameters, we consider a two-level EDFA model, which we extend to multiple signal and pump spatial modes, neglecting inhomogeneous broadening and amplified spontaneous emission. In this physical model the amplitude gains are

$$\gamma_{\mathrm{s},kk} = \frac{1}{2}\int_{-\infty}^{+\infty}\int_{-\infty}^{+\infty}(\sigma_e(\lambda_\mathrm{s})N_2(x,y,z) - \sigma_a(\lambda_\mathrm{s})N_1(x,y,z)) \cdot |\mathbf{\Psi}_{s,k}(x,y)|^2 dxdy, \quad (29)$$

$$\gamma_{p,m} = -\frac{1}{2}\int_{-\infty}^{+\infty}\int_{-\infty}^{+\infty}\sigma_a(\lambda_p)N_1(x,y,z)|\mathbf{\Psi}_{p,m}(x,y)|^2 dxdy, \quad (30)$$

where $\sigma_e(\lambda)$ and $\sigma_a(\lambda)$ are wavelength-dependent emission and absorption cross-sections; $N_1(x,y,z)$ and $N_2(x,y,z)$ are local erbium ion concentrations at lower and upper energy levels; $\mathbf{\Psi}_{\mathrm{s},k}(x,y)$ and $\mathbf{\Psi}_{p,m}(x,y)$ are normalized electric field distributions of the kth signal mode and mth pump mode, respectively. In our simulations we have used $\sigma_e = 3.63\times10^{-25}$ m^2 and $\sigma_a = 4.34\times10^{-25}$ m^2 at a signal wavelength of $\lambda_\mathrm{s} = 1550$ nm. Comparing (29) to (28) we can write down expressions for coupling coefficients $\gamma_{\mathrm{s},kl}$

$$\gamma_{\mathrm{s},kl} = \frac{1}{2}\int_{-\infty}^{+\infty}\int_{-\infty}^{+\infty}(\sigma_e(\lambda_s)N_2(x,y,z) - \sigma_a(\lambda_s)N_1(x,y,z)) \cdot \mathbf{\Psi}^*_{\mathrm{s},k}(x,y)\cdot\mathbf{\Psi}_{\mathrm{s},l}(x,y)\,dxdy. \quad (31)$$

We find the local concentrations of erbium ions at lower and upper energy levels by solving rate equations under the conditions of steady state regime. $N_1(x,y,z)$ and $N_2(x,y,z)$ are functions of erbium doping distribution $N_{\mathrm{Er}}(x,y,z)$, and local signal and pump intensities normalized to corresponding saturation intensities, and are given by

$$N_1(x,y,z) = N_{\mathrm{Er}}(x,y,z)\left(1 + \frac{I_\mathrm{s}(x,y,z)}{I_{\mathrm{s,sat}}} + \frac{I_\mathrm{p}(x,y,z)}{I_{\mathrm{p,sat}}}\right)^{-1} \cdot\left(1 + \frac{\sigma_e(\lambda_\mathrm{s})}{\sigma_e(\lambda_\mathrm{s}) + \sigma_a(\lambda_\mathrm{s})}\frac{I_\mathrm{s}(x,y,z)}{I_{\mathrm{s,sat}}}\right). \quad (32)$$

$$N_2(x,y,z) = N_{\mathrm{Er}}(x,y,z) - N_1(x,y,z). \quad (33)$$

The total local intensity at signal wavelength I_s is found by summing all the signal modes incoherently because the phase relationship between signal modes is randomized by fast data modulation in a fiber optic communication system with a characteristic speed much faster than excited erbium ion relaxation time. On the other hand, total local intensity at pump wavelength I_p is found by adding all the pump modes coherently because pump modes are unmodulated. Therefore, we have

$$I_s(x,y,z) = \sum_{k=1}^{D_s}|a_{\mathrm{s},k}(z)\,\mathbf{\Psi}_{\mathrm{s},k}(x,y)|^2. \quad (34)$$

$$I_p(x,y,z) = \left|\sum_{m=1}^{D_p}a_{\mathrm{p},m}(z)\,\mathbf{\Psi}_{\mathrm{p},m}(x,y)\right|^2. \quad (35)$$

The saturation intensities are given by

$$I_{\mathrm{s,sat}} = hc/[\lambda_s(\sigma_e(\lambda_s) + \sigma_a(\lambda_s))], \quad (36)$$

$$I_{\mathrm{p,sat}} = hc/(\lambda_p\sigma_a(\lambda_p)), \quad (37)$$

where h is the Planck's constant and c is the speed of light.

We now show that coupling between signal modes in MM-EDFA is negligible. For this purpose, consider the case of only two signal modes, which can be easily generalized to a higher number of modes. The coupled signal mode equations

are

$$\frac{da_{\mathrm{s},1}}{dz} = -j\beta_{\mathrm{s},1}a_{\mathrm{s},1} + \gamma_{\mathrm{s},11}a_{\mathrm{s},1} + \gamma_{\mathrm{s},12}a_{\mathrm{s},2}. \tag{38}$$

$$\frac{da_{\mathrm{s},2}}{dz} = -j\beta_{\mathrm{s},2}a_{\mathrm{s},2} + \gamma_{\mathrm{s},22}a_{\mathrm{s},2} + \gamma_{\mathrm{s},21}a_{\mathrm{s},1}. \tag{39}$$

To simplify the equations we can make a change of variables

$$a_{\mathrm{s},k} = \tilde{a}_{\mathrm{s},k}\exp\left(-j\beta_{\mathrm{s},k}z\right), \quad k = 1,\, 2 \tag{40}$$

and express the system of equations in the following matrix form

$$\begin{bmatrix} \dfrac{d\tilde{a}_{\mathrm{s},1}}{dz} \\ \dfrac{d\tilde{a}_{\mathrm{s},2}}{dz} \end{bmatrix} = \begin{bmatrix} \gamma_{\mathrm{s},11} & \gamma_{\mathrm{s},12}e^{j(\beta_{\mathrm{s},1}-\beta_{\mathrm{s},2})z} \\ \gamma_{\mathrm{s},21}e^{j(\beta_{\mathrm{s},2}-\beta_{\mathrm{s},1})z} & \gamma_{\mathrm{s},22} \end{bmatrix} \begin{bmatrix} \tilde{a}_{\mathrm{s},1} \\ \tilde{a}_{\mathrm{s},2} \end{bmatrix}, \tag{41}$$

which is a homogeneous system of linear differential equations. The solution can be expressed as

$$\begin{bmatrix} \tilde{a}_{\mathrm{s},1}\,(z) \\ \tilde{a}_{\mathrm{s},2}\,(z) \end{bmatrix} = J \begin{bmatrix} \tilde{a}_{\mathrm{s},1}\,(0) \\ \tilde{a}_{\mathrm{s},2}\,(0) \end{bmatrix}, \tag{42}$$

where J is given by the following matrix exponential

$$J = \exp \times \left(\begin{bmatrix} \displaystyle\int_0^z \gamma_{\mathrm{s},11}(\eta)d\eta & \displaystyle\int_0^z \gamma_{\mathrm{s},12}(\eta)e^{j(\beta_{\mathrm{s},1}-\beta_{\mathrm{s},2})\eta}d\eta \\ \displaystyle\int_0^z \gamma_{\mathrm{s},21}(\eta)e^{j(\beta_{\mathrm{s},2}-\beta_{\mathrm{s},1})\eta}d\eta & \displaystyle\int_0^z \gamma_{\mathrm{s},22}(\eta)d\eta \end{bmatrix} \right). \tag{43}$$

Using the definition of a matrix exponential we can express J as

$$J = \sum_{k=0}^{+\infty} \frac{1}{k!} \times \begin{bmatrix} \displaystyle\int_0^z \gamma_{\mathrm{s},11}(\eta)d\eta & \displaystyle\int_0^z \gamma_{\mathrm{s},12}(\eta)e^{j\left(\beta_{\mathrm{s},1}-\beta_{\mathrm{s},2}\right)\eta}d\eta \\ \displaystyle\int_0^z \gamma_{\mathrm{s},21}(\eta)e^{j\left(\beta_{\mathrm{s},2}-\beta_{\mathrm{s},1}\right)\eta}d\eta & \displaystyle\int_0^z \gamma_{\mathrm{s},22}(\eta)d\eta \end{bmatrix}^k. \tag{44}$$

From this expression we see that off-diagonal elements of J, which represent mode coupling in MM-EDFA, are given by linear combinations of terms of the following form

$$\int_0^z \gamma_{\mathrm{s},kl}(\eta)e^{i(\beta_{\mathrm{s},k}-\beta_{\mathrm{s},l})\eta}d\eta, \qquad k \neq l. \tag{45}$$

These integrals are much smaller in magnitude than the diagonal elements of the exponent matrix. This is due to the fact that the complex exponential term in (45) oscillates very rapidly with a frequency equal to the longitudinal spatial beat frequency between the pair of signal modes. The beat length is typically much shorter than the characteristic length over which coupling coefficients $\gamma_{\mathrm{s},kl}$ change considerably. This causes the integrand to quickly oscillate between positive and negative values, thereby significantly reducing the magnitude of the integral. Therefore, mode coupling between signal modes can be neglected in MM-EDFA. Using the same argument we can also show that coupling between pump modes can be neglected in MM-EDFA.

It should be noted, however, that in a transmission fiber hundreds to thousands of kilometers long, coupling between signal modes can be significant. This is due to random index perturbations, corresponding to random fluctuations of $\varepsilon - \varepsilon_u$, which affect the coupling coefficients $\gamma_{\mathrm{s},kl}$. Unlike the case of a MM-EDFA, the correlation length is much shorter than the transmission fiber length and hence, $\gamma_{\mathrm{s},kl}$ in (45) behaves like a random process that decorrelates over a length scale much shorter than the transmission fiber length. As a result, the integrand in (45) does not oscillate rapidly, and instead of averaging out, the integral accumulates to a nonzero value in a statistical way [14].

REFERENCES

[1] R.-J. Essiambre, G. Kramer, P. J. Winzer, G. J. Foschini, and B. Goebel, "Capacity limits of optical fiber networks," *J. Lightw. Technol.*, vol. 28, no. 4, pp. 662–701, Feb. 2010.

[2] P. J. Winzer and G. J. Foschini, "MIMO capacities and outage probabilities in spatially multiplexed optical transport systems," *Opt. Exp.*, vol. 19, no. 17, pp. 16680–16696, Aug. 2011.

[3] P. J. Winzer, "Spatial multiplexing: The next frontier in network capacity scaling," presented at Eur. Conf. Exhib. Opt. Commun., London, U.K., 2013, Paper We.1.D.1.

[4] K.-P. Ho and J. M. Kahn, "Statistics of group delays in multimode fiber with strong mode coupling," *J. Lightw. Technol.*, vol. 29, no. 21, pp. 3119–3128, Nov. 2011.

[5] K.-P. Ho and J. M. Kahn, "Mode-dependent loss and gain: Statistics and effect on mode-division multiplexing," *Opt. Exp.*, vol. 19, no. 17, pp. 16612–16635, Aug. 2011.

[6] D. Askarov and J. M. Kahn, "Design of transmission fibers and doped fiber amplifiers for mode-division multiplexing," *IEEE Photon. Technol. Lett.*, vol. 24, no. 21, pp. 1945–1948, Nov. 2012.

[7] G. L. Cocq, L. Bigot, A. L. Rouge, M. Bigot-Astruc, P. Sillard, and Y. Quiquempois, "Design and characterization of a multimode EDFA supporting 4 transverse mode groups for modal division multiplexed transmissions," presented at the Eur. Conf. Exhib. Opt. Commun., Amsterdam, The Netherlands, 2012, Paper Tu.3.F.4.

[8] N. Bai, E. Ip, T. Wang, and G. Li, "Multimode fiber amplifier with tunable modal gain using a reconfigurable multimode pump," *Opt. Exp.*, vol. 19, no. 17, pp. 16601–16611, Aug. 2011.

[9] J. K. Bae, J. Bae, S. H. Kim, N. Park, and S. B. Lee, "Dynamic EDFA gain-flattening filter using two LPFGs with divided coil heaters," *IEEE Photon. Technol. Lett.*, vol. 17, no. 6, pp. 1226–1228, Jun. 2005.

[10] R. Y. Gu, E. Ip, M.-J. Li, Y. K. Huang, and J. M. Kahn, "Experimental demonstration of spatial light modulator few-mode fiber switch for space-division multiplexing," presented at the Frontier Opt., Orlando, FL, USA, 2013, Paper FW6B.4.

[11] K.-P. Ho and J. M. Kahn, "Frequency diversity in mode-division multiplexing systems," *J. Lightw. Technol.*, vol. 29, no. 24, pp. 3719–3726, Dec. 2011.

[12] S. Randel, R. Ryf, C. Schmidt, M. A. Mestre, P. J. Winzer, and R. J. Essiambre, "MIMO processing for space-division multiplexed transmission," presented at the Adv. Photon. Congr., Colorado Springs, CO, USA, 2012, Paper SpW3B.4.

[13] Y. Jung, S. Alam, Z. Li, A. Dhar, D. Giles, I. P. Giles, J. K. Sahu, F. Poletti, L. Grüner-Nielsen, and D. J. Richardson, "First demonstration and detailed characterization of a multimode amplifier for space division multiplexed transmission systems," *Opt. Exp.*, vol. 19, no. 26, pp. B952–B957, Dec. 2011.

[14] K.-P. Ho and J. M. Kahn, "Mode coupling and its impact on spatially multiplexed systems," in *Optical Fiber Telecommunications VI*, I. P. Kaminow, T. Li, and A. E. Willner, Eds. Amsterdam, The Netherlands: Elsevier, 2013.

[15] K.-P. Ho and J. M. Kahn, "Delay-spread distribution for multimode fiber with strong mode coupling," *IEEE Photon. Technol. Lett.*, vol. 24, no. 21, pp. 1906–1909, Nov. 2012.

[16] B. Inan, B. Spinnler, F. Ferreira, D. van den Borne, A. Lobato, S. Adhikari, V. A. J. M. Sleiffer, M. Kuschnerov, N. Hanik, and S. L. Jansen, "DSP complexity of mode-division multiplexed receivers," *Opt. Exp.*, vol. 20, no. 9, pp. 10859–10869, Apr. 2011.
[17] S. Ö. Arik, D. Askarov, and J. M. Kahn, "Effect of mode coupling on signal processing complexity in mode-division multiplexing," *J. Lightw. Technol.*, vol. 31, no. 3, pp. 423–431, Feb. 2013.
[18] E. Ip, M.-J. Li, W. Wood, J. Hu, and Y. Yano, "Temporal variations in the channel matrix in few-mode fiber recirculating loop transmission," presented at the Proc. IEEE Summer Topical Space Division Multiplexing Opt. Comm., Waikoloa, HI, USA, Jul. 2013, Paper WC2.2.
[19] N. Cvijetic, E. Ip, N. Prasad, and M.-J. Li, "Experimental frequency-domain channel matrix characterization for SDM-MIMO-OFDM systems," presented at the Proc. IEEE Summer Topical Space Division Multiplexing Opt. Comm., Waikoloa, HI, USA, Jul. 2013, Paper WC4.3.
[20] S. Ö. Arik, D. Askarov, and J. M. Kahn, "Adaptive frequency-domain equalization in mode-division multiplexing systems," *J. Lightwave Technol.*, vol. 32, no. 10, pp. 1841–1852, 2014.
[21] R. A. Panicker and J. M. Kahn, "Algorithms for compensation of multimode fiber dispersion using adaptive optics," *J. Lightw. Technol.*, vol. 27, no. 24, pp. 5790–5799, Dec. 2009.
[22] R. N. Mahalati, D. Askarov, J. P. Wilde, and J. M. Kahn, "Adaptive control of input field to achieve desired output intensity profile in multimode fiber with random mode coupling," *Opt. Exp.*, vol. 20, no. 13, pp. 14321–14337, 2012.
[23] D. Marcuse, *Theory of Dielectric Optical Waveguides* 2nd ed., Boston, MA, USA: Academic, 1991.
[24] E. Desurvire, *Erbium-Doped Amplifiers Principles and Application,* New York, NY, USA: Wiley, 1994.

Reza Nasiri Mahalati received the B.S. degree in electrical engineering from the Sharif University of Technology, Tehran, Iran, in 2008, and the M.S. and Ph.D. degrees in electrical engineering from Stanford University, Stanford, CA, USA, in 2010 and 2013, respectively.

His current research interests include mode-division multiplexing, fiber-based imaging, optimization, and digital signal processing.

Daulet Askarov received the B.S. degree in applied mathematics and physics from the Moscow Institute of Physics and Technology, Moscow, Russia, in 2009, and the M.S. degree in electrical engineering from Stanford University, Stanford, CA, USA, in 2011, where he is currently working toward the Ph.D. degree in electrical engineering.

His current research interests include various topics in multimode fiber communications.

Joseph M. Kahn (M'90–SM'98–F'00) received the A.B., M.A., and Ph.D. degrees in physics from University of California, Berkeley, CA, USA,U.C. Berkeley in 1981, 1983, and 1986, respectively.

From 1987–1990, he was at AT&T Bell Laboratories, Crawford Hill Laboratory, Holmdel, NJ, USA. He demonstrated multi-Gbit/s coherent optical fiber transmission systems, setting world records for receiver sensitivity. From 1990–2003, he was in the faculty of the Department of Electrical Engineering and Computer Sciences at U.C. Berkeley, performing research on optical and wireless communications. Since 2003, he has been a Professor of Electrical Engineering at Stanford University, Stanford, CA, USA, where he heads the Optical Communications Group. His current research interests include: fiber-based imaging, spatial multiplexing, rate-adaptive and spectrally efficient modulation and coding methods, coherent detection and associated digital signal processing algorithms, digital compensation of fiber nonlinearity, and free-space systems. In 2000, he helped found StrataLight Communications, where he served as Chief Scientist from 2000–2003. StrataLight was acquired by Opnext, Inc. in 2009.

Dr. Kahn received the National Science Foundation Presidential Young Investigator Award in 1991. From 1993–2000, he served as a Technical Editor of IEEE *Personal Communications Magazine*. Since 2009, he has been an Associate Editor of IEEE/OSA JOURNAL OF OPTICAL COMMUNICATIONS AND NETWORKING.